Stability and Local Unfolding of SOD1 in the Presence of Protein Crowders

Anna Bille,[†,§] Kristine Steen Jensen,[‡,§] Sandipan Mohanty,[¶] Mikael Akke,[*,‡] and Anders Irbäck[*,†]

†*Computational Biology and Biological Physics, Department of Astronomy and Theoretical Physics, Lund University, Sölvegatan 14A, SE-223 62 Lund, Sweden*

‡*Department of Biophysical Chemistry, Center for Molecular Protein Science, Lund University, P.O. Box 124, SE-22100 Lund, Sweden*

¶*Institute for Advanced Simulation, Jülich Supercomputing Centre, Forschungszentrum Jülich, D-52425 Jülich, Germany*

§*These authors contributed equally.*

E-mail: mikael.akke@bpc.lu.se; anders@thep.lu.se

Abstract

Using NMR and Monte Carlo (MC) methods, we investigate the stability and dynamics of superoxide dismutase 1 (SOD1) in homogeneous crowding environments, where either bovine pancreatic trypsin inhibitor (BPTI) or the B1 domain of streptococcal protein G (PGB1) serves as a crowding agent. By NMR, we show that both crowders, and especially BPTI, cause a drastic loss in the overall stability of SOD1 in its apo monomeric form. Additionally, we determine chemical shift perturbations indicating that SOD1 interacts with the crowder proteins in a residue-specific manner that further depends on the identity of the crowding protein. Furthermore, the specificity of SOD1-crowder interactions is reciprocal: chemical shift perturbations on BPTI and PGB1 identify regions that interact preferentially with SOD1. By MC simulations, we investigate the local unfolding of SOD1 in the absence and presence of the crowders. We find that the crowders primarily interact with the long flexible loops of the folded SOD1 monomer. The basic mechanisms by which the SOD1 β-barrel core unfolds remain unchanged when adding the crowders. In particular, both with and without the crowders, the second β-sheet of the barrel is more dynamic and unfolding-prone than the first. Notably, the MC simulations (exploring the early stages of SOD1 unfolding) and the NMR experiments (under equilibrium conditions) identify largely the same set of PGB1 and BPTI residues as prone to form SOD1 contacts. Thus, contacts stabilizing the unfolded state of SOD1 in many cases appear to form early in the unfolding reaction.

1 Introduction

Unfolding, misfolding and aggregation of Cu,Zn-binding superoxide dismutase 1 (SOD1) have been linked to the fatal motor neuron disease amyotrophic lateral sclerosis (ALS).[1,2] Consequently, a great body of research has focused on the unfolding process of SOD1.[3–7] Unlike the highly stable Cu,Zn-bound homodimeric native form of SOD1, apo monomeric SOD1 is only marginally stable[8,9] and a potential starting point for aggregation. The mechanisms of SOD1 misfolding have been extensively studied in dilute solution, and recently also in cellular environments. In particular, recent studies of the SOD1 folding-unfolding equilibrium in live cells have indicated that the cellular environment stabilizes the unfolded state via transient, presumably sequence-specific interactions with cellular proteins.[10,11] Protein destabilization in dense systems is contrary to what one would expect if purely steric effects dominated, but seems to be common in simple homogeneous protein crowder environments.[11–14] However, the mechanisms by which surrounding macromolecules may cause a destabilization remain incompletely understood.

The conformational dynamics of SOD1 under dilute conditions have been extensively studied by computational methods such as molecular dynamics,[15–18] discrete molecular dynamics,[19–21] MC,[22] mechanical response analysis,[23–25] and bioinformatics-based techniques.[26] However, as far as we know, there have been no previous simulations of SOD1 in the presence of macromolecular crowders.

In this article, we use NMR experiments and MC simulations to investigate the effects of two destabilizing crowder proteins, BPTI and PGB1, on the reduced apo SOD1 monomer (referred to simply as SOD1 in the rest of the paper). BPTI and PGB1 share the advantage of being small, highly stable and highly soluble, which facilitates both simulations and NMR experiments. By NMR, we show that indeed both these crowder proteins, and especially BPTI, have a destabilizing effect on SOD1. Additionally, we obtain chemical shift perturbations indicating that unfolded SOD1 and the crowder proteins interact in a residue-specific manner. By MC, we study the local unfolding of SOD1 through simulations started with SOD1 in its folded state. We find that the crowder molecules mainly interact with the long flexible loops of

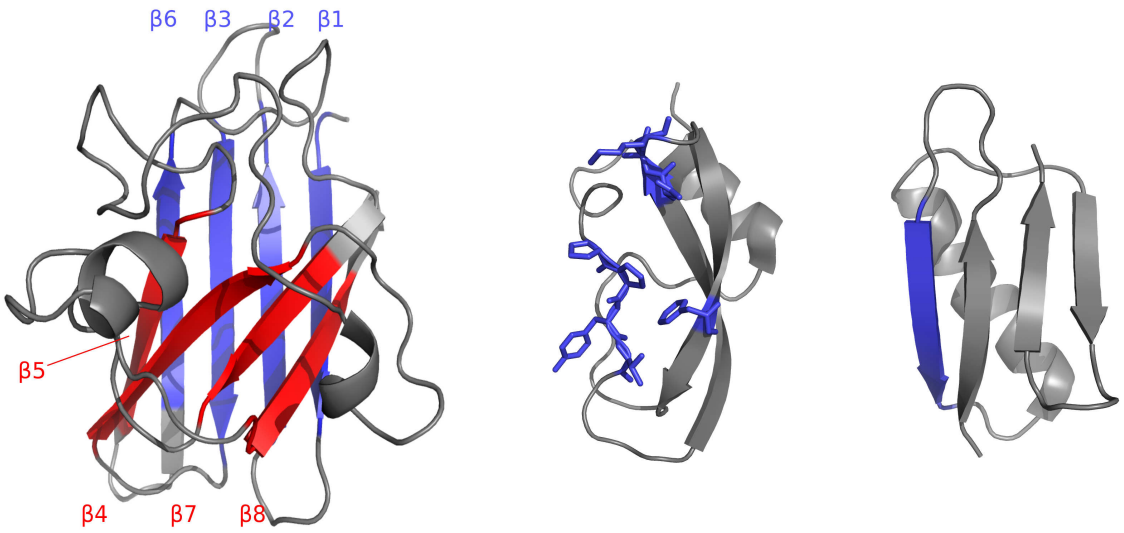

Figure 1: Schematic folds for (from left to right) SOD1 (PDB ID 2V0A), BPTI (4PTI) and PGB1 (2GB1). In SOD1, the first β-sheet (strands $\beta1$, $\beta2$, $\beta3$ and $\beta6$) is indicated in blue and the second ($\beta5$, $\beta4$, $\beta7$ and $\beta8$) in red. In BPTI and PGB1, blue color indicates the regions most prone to form contacts with SOD1 in our simulations (see Results). These regions are the edge strand $\beta2$ (residues 14–19) of PGB1 and a sticky patch with two prolines on the BPTI surface (comprising residues P8, P9, Y10, T11, N24, A25, K26 and F33). The structures are model approximations derived from the respective PDB structures by MC with minimization. Drawn with PyMOL.[27]

SOD1, and no sign that their presence would speed up unfolding or cause any major changes in how the SOD1 β-barrel core unfolds. The simulations therefore suggest that the main reason for the experimentally observed destabilization is slower folding rather than faster unfolding in the presence of the protein crowders. This conclusion is in agreement with the detected interactions between crowders and unfolded SOD1, which serve to stabilize the unfolded state.

2 Experimental and Computational Methods

This section describes our MC simulations and NMR experiments. Illustrations of SOD1 and our two crowder proteins, PGB1 and BPTI, can be found in Figure 1. The SOD1 fold has a β-barrel core composed of eight strands, $\beta1$–$\beta8$ (residues 2–9, 15–22, 29–36, 41–48, 83–89, 95–101, 116–120 and 143–148), and two long loops, called the zinc-binding (49–83) and electrostatic (121–142) loops. In the native SOD1 dimer, each unit contains one disulfide bond. Throughout this paper, we study the disulfide-reduced apo monomer.

2.1 Biophysical Model

The simulated systems consist of one SOD1 molecule and eight PGB1 or BPTI molecules, enclosed in a cubic periodic box with side length 66 Å. This setup yields crowder densities ($\sim$300 mg/mL) comparable to estimated macromolecule densities in *Escherichia coli* ($\sim$300–400 mg/mL).[28] The volume fraction occupied by crowders is $\sim$20 %. The simulation temperature is 47°C, which is slightly above the experimental melting temperature of SOD1.[8,9] For reference, crowder-free simulations of SOD1 are also performed, using the same temperature.

The simulations are carried out using an all-atom protein representation with torsion angles as the degrees of freedom, along with an implicit solvent force field.[29] A detailed description of the interaction potential can be found elsewhere.[29] Previous work based on this model include folding/unfolding studies of SOD1[22] and several other proteins with >90 residues.[30–34] Recently, it was used by us to study peptide folding in the presence of PGB1 and BPTI crowders.[35–37]

Our simulations use the same fully atomistic representation for both SOD1 and the crowder proteins. However, because of their high thermal stability,[38,39] the PGB1 and BPTI crowder proteins are modeled with a fixed backbone. Their only internal degrees of freedom are side-chain rotations. The assumed backbone conformations of BPTI and PGB1 are model approximations of the PDB structures 4PTI and 2GB1, with root-mean-square deviations (RMSDs) of $\lesssim$1 Å from these structures (calculated over backbone and C_β atoms).

2.2 MC Sampling Methods

The systems described above are simulated using constant-temperature MC methods. Only "small-step" elementary MC updates are included in the move set, to ensure that the system cannot artificially jump between different free-energy minima, without having to climb intervening barriers. With this restriction, the simulations should capture basics of the long-time dynamics.[40]

The move set employed has the following components: (i) the semi-local Biased Gaussian Steps (BGS) method[41] for backbone angles (only for SOD1), (ii) standard Metropolis

rotations of side-chain angles, and (iii) small rigid-body motions of whole chains (translations and rotations). The "time" unit of the simulations is MC cycles. The number of attempted elementary updates in one MC cycle is set equal to the number of degrees of freedom (649 for the crowder-free system, 1783 with BPTI crowders, and 1903 with PGB1 crowders). With this choice, the average number of attempted internal updates of SOD1 in one MC cycle is the same for all three systems. The parameters of the updates are tuned so as to have an acceptance rate of 45–50%. The two parameters of the BGS move, which govern the overall step size and the degree of bias toward local deformations, are set to $a = 2000$ rad^{-2} and $b = 500$ (rad/Å)^2.

All simulations are run with the program PROFASI,[42] using both vector and thread parallelization. For each system, a set of about 100 independent runs is generated (99 without crowders, 123 with PGB1 crowders, 124 with BPTI crowders). Each run comprises 5×10^6 MC cycles.

Our initial ensemble of SOD1 structures was created starting from the experimental structure in Figure 1, which is for the dimeric form. The SOD1 monomer has flexible loops.[43] Therefore, to thermalize the loops, long preparatory runs ($\sim 10^6$ MC cycles) were performed, using a restricted move set to ensure preservation of the β-barrel core, before starting the production runs.

2.3 Analysis of MC Data

To assess the foldedness of the SOD1 β-barrel core, we compute an RMSD over the 57 β-barrel residues, Δ^{barrel}. To remove short-time fluctuations, each trajectory is split into 20 time bins of size 0.25×10^6 MC cycles, and an average of Δ^{barrel}, $\bar{\Delta}^{\text{barrel}}$, is computed for each time bin.

To monitor local changes in the β-barrel structure, we compute a restricted two-strand RMSD, Δ^{ij}, for each of the eight pairs i, j of neighboring strands. The foldedness of individual strands is quantified based on C_α-C_α contacts among the 57 β-barrel residues. For a given residue i, let A_i denote the set of residues j with $|i - j| > 2$ whose C_α-C_α distance s_{ij} from residue i is <6 Å in the folded structure. With this definition, the foldedness of strand k, Q_k,

is calculated as[44]

$$Q_k = \sum_{i \in \mathrm{S}_k} \sum_{j \in \mathrm{A}_i} \mathrm{e}^{-(r_{ij}-s_{ij})^2/\xi^2} \Big/ \sum_{i \in \mathrm{S}_k} |\mathrm{A}_i| \tag{1}$$

where S_k is the set of residues in strand k, the r_{ij}'s are C_α-C_α distances, ξ is a parameter set to 3 Å, and $|\mathrm{A}_i|$ denotes the size of set A_i.

To investigate how SOD1 interacts with the crowder molecules, intermolecular residue-residue contact frequencies are computed. Two residues are defined in contact if their C_α atoms are within 8 Å from each other.

Secondary structure is classified using the STRIDE program.[45]

2.4 Protein Expression and Purification

A plasmid with cDNA of hSOD1 C6A/F50E/G51E/C57S/ C111A/C146S (pwtSOD1$^{\Delta C}$) in pET17b (synthesized by GenScript) was used for expression in *E. coli* BL21(DE3) pLysS cells.[46] The cysteine-free variant pwtSOD1$^{\Delta C}$ mimics the reduced apo state of SOD1. Uniformly ^{15}N-labeled pwtSOD1$^{\Delta C}$ were produced by first cultivating in LB medium supplemented with ampicillin (100 μg/mL) and chloramphenicol (35 μg/mL) to OD_{600}=0.8 at 37°C, with rigorous aeration. Then the cells were suspended in M9 medium supplemented with 1.5 g/L $^{15}NH_4Cl$ (Cambridge Isotopes Laboratories, Inc.), 4 g/L glucose, ampicillin (100 μg/mL) and chloramphenicol (35 μg/mL) and left for expression for 1 h at 37°C, with rigorous aeration, before 0.7 mM of IPTG (Sigma) was added along with 30 μM each of $ZnCl_2$ and $CuSO_4$. Cultures were left for overnight expression at 25°C, with aeration. pwtSOD1$^{\Delta C}$ was purified essentially as previously described.[47] Monomeric pwtSOD1$^{\Delta C}$ was isolated by a final size exclusion chromatography step on a Superdex 75 analytical column (GE Healthcare) in 10 mM $NaPO_4$ and concentrated through spin filters MWCO 10,000 (Millipore) directly before the NMR experiments. Sample concentrations were estimated by absorbance measurement at 280 nm on a NanoDrop 2000/2000c spectrophotometer (Thermo Scientific) using an extinction coefficient of 5500 $M^{-1}cm^{-1}$.

PGB1 was expressed as a variant including the mutations T2Q, N8D and N37D (PGB1-QDD), which mitigate sample degradation, and purified essentially as described[48,49] in non-

labeled and ^{13}C,^{15}N-labeled forms. Non-labeled PGB1-QDD was used as crowding agent in a sample with pwtSOD1$^{\Delta C}$, whereas ^{13}C,^{15}N-labeled PGB1-QDD was used in control experiments without pwtSOD1$^{\Delta C}$ to measure chemical shifts of PGB1-QDD alone at high protein concentration. Following 25x dilution of the samples into NMR buffer, the final sample concentrations were estimated by absorbance measurement at 280 nm on a NanoDrop 2000/2000c spectrophotometer (Thermo Scientific) using an extinction coefficient of 9970 $M^{-1}cm^{-1}$.

Bovine pancreatic trypsin inhibitor (BPTI) (97% purity by HPLC from Bayer HealthCare AG, Wuppertal, Germany) was dissolved in milli Q water and dialysed extensively against milli Q water (MWCO 3500, Spectrum Laboratories, Inc.) before the sample was flash frozen in a dry ice/ethanol bath and lyophilized.

2.5 NMR Sample Preparation

NMR samples were prepared in 10 mM Na-PO_4, 1 mM EDTA, pH 7.0, 10% (v/v) D_2O. Lyophilized PGB1 or lyophilized BPTI was dissolved in a ^{15}N pwtSOD1$^{\Delta C}$ sample. The final volume of the very viscous samples was adjusted to obtain 48 mM (300 mg/mL) PGB1 or BPTI and 1 mM pwtSOD1$^{\Delta C}$. The final concentrations of the ^{13}C,^{15}N-labeled PGB1-QDD samples were 21 mM (130 mg/mL) and 10.7 mM (66 mg/mL). The pH was adjusted to 7.0 with the addition of μL amounts of 0.05 M NaOH or HCl.

2.6 NMR Experiments

Backbone chemical shifts were determined from ^{1}H-^{15}N HSQC experiment at 5, 10, 15, 20, 25, 30, 35, 37, 40, 45, 47, 50, 55, 60 and 65°C on a Varian/Agilent VNMRS DirectDrive spectrometer operating at a static magnetic field strength of 11.7 T and equipped with a triple resonance probe.

2.7 Analysis of NMR Data

Spectra were processed in NMRPipe[50] and analyzed in CcpNMR Analysis.[51] Chemical shift perturbations ($\Delta\delta$) of individual residues were determined as

$$\Delta\delta = [(\delta^1\mathrm{H_A} - \delta^1\mathrm{H_B})^2 + 0.15 \times (\delta^{15}\mathrm{N_A} - \delta^{15}\mathrm{N_B})^2]^{1/2} \quad (2)$$

For PGB1-QDD, two chemical shift perturbations were calculated: $\Delta\delta_{\mathrm{SOD1}}$, where A and B indicate samples with and without 1 nM pwtSOD1$^{\Delta\mathrm{C}}$ added, respectively, and where the PGB1-QDD concentration was 48 mM in A and 21 mM in B; and $\Delta\delta_{\mathrm{conc}}$, where A and B indicate samples with only PGB1-QDD at concentrations of 21 mM and 11 mM, respectively. For BPTI, $\Delta\delta_{\mathrm{SOD1}}$ values were calculated using eq 2 with A and B indicating samples with and without 1 mM pwtSOD1$^{\Delta\mathrm{C}}$, and with a BPTI concentration of 46 mM in both cases. Finally, for pwtSOD1$^{\Delta\mathrm{C}}$, $\Delta\delta_{\mathrm{PGB1}}$ values were calculated using eq 2 with A and B indicating samples with and without 48 mM PGB1-QDD and with 1 mM pwtSOD1$^{\Delta\mathrm{C}}$ in both cases.

The populations of folded and unfolded pwtSOD1$^{\Delta\mathrm{C}}$ were determined from the cross peaks of the C-terminal Q153 residue.[11]

3 Results and Discussion

Our study of the impact of PGB1 and BPTI crowders on SOD1 can be divided into two parts. We first investigate equilibrium properties of the systems, through NMR measurements. We then turn to local unfolding properties of SOD1, studied by MC simulations started with SOD1 in its folded state.

3.1 SOD1 Stability from NMR Experiments

Using NMR, we investigated the effects of PGB1-QDD and BPTI crowders on the stability of pwtSOD1$^{\Delta\mathrm{C}}$. In contrast to what is expected with purely steric crowders, we find that both BPTI and PGB1-QDD crowders have a destabilizing effect on pwtSOD1$^{\Delta\mathrm{C}}$. Figure 2 shows the temperature dependence of the folded population of pwtSOD1$^{\Delta\mathrm{C}}$, as estimated from the

relative intensity of the cross peaks of the C-terminal Q153 residue in the folded and unfolded states.[11] Inspection shows that the behavior of these peaks is strongly correlated with that of other peaks at the higher temperatures (>40°C) where SOD1 is essentially fully unfolded. Therefore, although local in character, this parameter reports on global conformational changes. However, in the presence of PGB1-QDD and at lower temperatures (<40°C), the peak from the side chain indole of W32, located in strand β3, indicates that this part of the structure is more stable than the C-terminal strand β8 (Figure S1), suggesting that local unfolding might be at play under these conditions. As can be seen from Figure 2, in the absence of crowders, pwtSOD1$^{\Delta C}$ undergoes thermal unfolding at approximately 40°C, which is in line with previous work.[8,9] When adding BPTI or PGB1-QDD crowders, a drastic loss of stability is observed. In fact, with BPTI as crowding agent, the folded population of pwtSOD1$^{\Delta C}$ is negligible at all temperatures, as evidenced by the fact that no Q153 cross peak from the folded population is detectable in the spectra. By contrast, when PGB1-QDD is used as crowding agent, there still is a non-negligible folded population of SOD1 at low temperatures, but its maximum value, attained at 20°C, is as low as ≈40%. We note that the data in the presence of PGB1-QDD reveal both cold and heat denaturation of SOD1, similar to previous results.[11] Hence, the (partially) unfolded population is more than 50% at all temperatures with any of the two crowders.

3.2 Chemical Shift Perturbations Reveal Contacts between SOD1 and Crowders

We mapped interactions between pwtSOD1$^{\Delta C}$ and the crowder proteins at the residue level by analyzing chemical shift perturbations in the ^{1}H-^{15}N HSQC spectrum. Folded pwtSOD1$^{\Delta C}$ could not be studied in the presence of BPTI. However, the spectrum of folded pwtSOD1$^{\Delta C}$ at 20° reveals chemical shift perturbations in the presence of PGB1-QDD, with the largest effects observed for residues located in loop regions and edge strands (Figure S2). Next, by comparing the spectrum of unfolded pwtSOD1$^{\Delta C}$ in the absence of crowders with the spectra in the presence of either BPTI or PGB1-QDD, we identify chemical shift changes

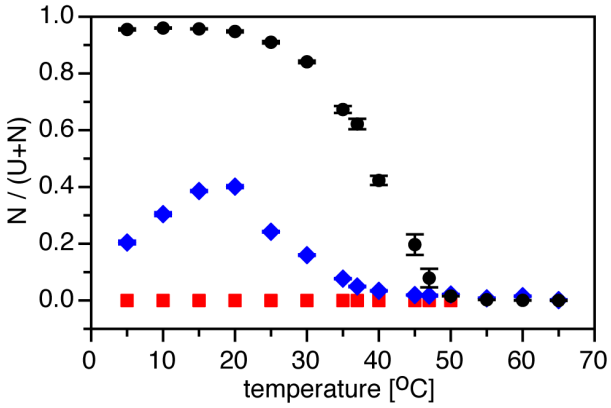

Figure 2: Temperature dependence of the folded population of pwtSOD1$^{\Delta C}$ from NMR measurements in three environments: without crowders (black circles), with BPTI crowders (red squares), and with PGB1 crowders (blue diamonds). The folded population is estimated from the relative intensity of the cross peaks from the folded and unfolded states of the C-terminal Q153 residue.[11] Error bars indicate the estimated standard error of the peak intensities obtained by error propagation of the standard deviation of the baseplane noise.

for several peaks. Apparently, there are interactions between unfolded pwtSOD1$^{\Delta C}$ and the crowder proteins that shift the folding-unfolding equilibrium by stabilizing the unfolded state. We note that the chemical shift changes are partially different in the spectra with BPTI or PGB1-QDD (Figure S3). In many cases the same peak moves but to different extents, whereas in other cases one peak moves with one crowder relative to no-crowding conditions and is absent in the presence of the other crowder. While the spectrum of unfolded pwtSOD1$^{\Delta C}$ is not fully assigned, we could identify certain residue segments that show chemical shift perturbations in the presence of crowders. Notably, these segments include residues T88-E100, corresponding to β5-loop V-β6 in the folded structure, and the C-terminal end of β8 (Figure S3). These results indicate that there are residue-specific interactions between unfolded pwtSOD1$^{\Delta C}$ and the crowders, similar to conclusions reached previously from in-cell NMR studies.[10,11]

Both crowder proteins stay folded across the entire temperature range studied here. For PGB1-QDD, we could obtain residue-level data on its interaction with pwtSOD1$^{\Delta C}$ throughout the temperature range. For BPTI, this was only possible at higher temperatures (>37°C) due to its propensity to form decamers,[52,53] which leads to severe line broadening of the NMR signals. Consistent with these results, we found in previous simulations that the amount of

crowder-crowder contacts are higher with BPTI than with PGB1-QDD crowders.[36]

Chemical shifts of PGB1-QDD were acquired both in the presence and absence of pwtSOD1$^{\Delta C}$, under otherwise nearly identical conditions; the PGB1-QDD concentrations differed by roughly a factor of 2 (see Methods). Figure 3c shows the measured pwtSOD1$^{\Delta C}$-induced chemical shift perturbations $\Delta\delta_{\mathrm{SOD1}}$ (eq 2) in PGB1-QDD at the different temperatures used. Because the measured chemical shift values are population-weighted averages of free and SOD1-bound PGB1-QDD, and the concentration of PGB1-QDD is 20-fold higher than that of pwtSOD1$^{\Delta C}$, we expect that the chemical shift difference between free and SOD1-bound PGB1-QDD is considerably higher than the values measured in the present experiments. The latter shift differences can be estimated from the present results to be maximally 2–4 ppm, which is in line with perturbations expected upon protein-protein interactions[54] and local unfolding.[55]

In Figures 3a,b, the $\Delta\delta_{\mathrm{SOD1}}$ data at two of the temperatures are mapped onto the three-dimensional structure of PGB1-QDD. Notably, we observe that the edge strand $\beta 2$ has relatively high $\Delta\delta_{\mathrm{SOD1}}$ values. At 20°C, there are also two residues with elevated $\Delta\delta_{\mathrm{SOD1}}$ in strand $\beta 4$. Nevertheless, among the four strands, the indications of interaction with pwtSOD1$^{\Delta C}$ are clearest for $\beta 2$. Additionally, an elevated $\Delta\delta_{\mathrm{SOD1}}$ is observed for residue D37 in the segment connecting the α-helix and the $\beta 3$ strand (Figure S4). This is one of the three mutated residues that differ from the wild-type sequence (N37D) used in the simulations. The D37 side chain has a significantly upshifted pK_a of 6.5,[49,56] making the chemical shifts of this residue highly sensitive to slight changes in pH around 6–7. Thus, the observed $\Delta\delta_{\mathrm{SOD1}}$ might arise from minor mismatches in pH between samples. Furthermore, we observe a large change in chemical shift for this residue upon dilution of the PGB1-QDD concentration that might reflect direct PGB1-PGB1 contacts or changes in the electrostatic potential due to self-screening. Figure 3d shows the chemical shift perturbations, $\Delta\Delta\delta = \Delta\delta_{\mathrm{SOD1}} - \Delta\delta_{\mathrm{conc}}$, that have been corrected for PGB1-PGB1 interactions.

We also characterized differences in BPTI chemical shifts with or without pwtSOD1$^{\Delta C}$. The peak intensities from BPTI are significantly lower than those from PGB1 due to the lower concentration of monomeric BPTI, making the analysis more challenging in this case. To

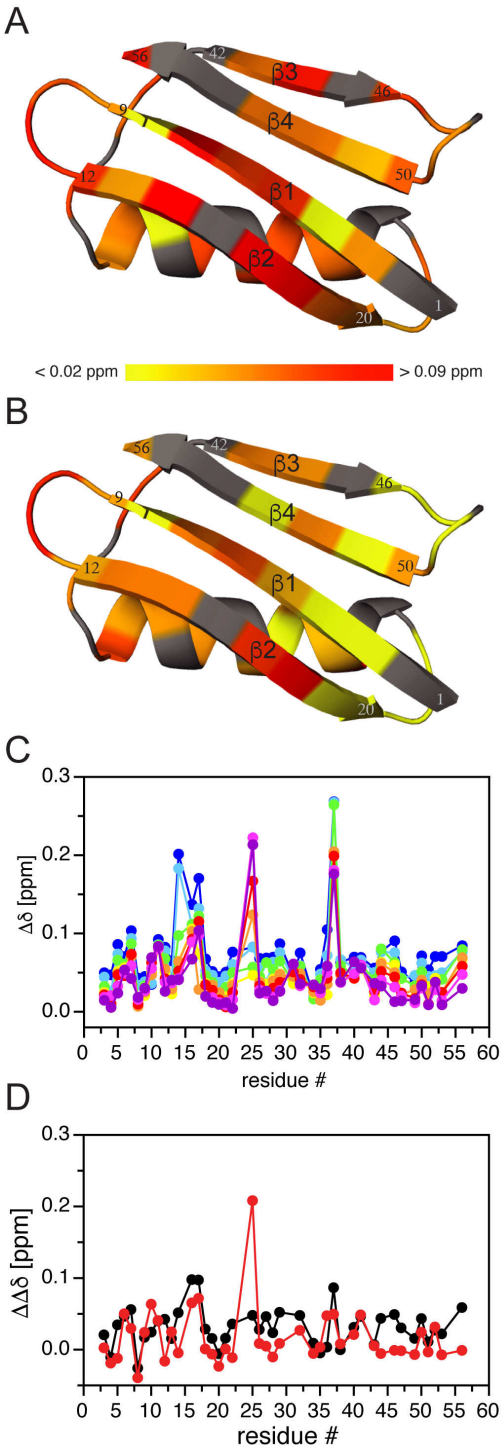

Figure 3: Continued on the following page.

Figure 3: Chemical shift perturbations in PGB1 upon interaction with SOD1. (A) Data for $\Delta\delta_{\mathrm{SOD1}}$ (eq 2) acquired at 20°C. (B) Data for $\Delta\delta_{\mathrm{SOD1}}$ acquired at 45°C. In panels A and B, data are color coded as indicated by the color gradient at the bottom of panel A, ranging from $\Delta\delta_{\mathrm{SOD1}} < 0.02$ ppm (yellow) to $\Delta\delta_{\mathrm{SOD1}} > 0.09$ ppm (red). Due to overlap with pwtSOD1$^{\Delta\mathrm{C}}$ resonances, 12 residues (2, 15, 23, 24, 30, 33, 39, 42, 45, 48, 54 and 55) in PGB1-QDD were difficult to identify uniquely in the pwtSOD1$^{\Delta\mathrm{C}}$ + PGB1-QDD spectra and therefore left out of the analysis (gray). In addition, one residue (D37) was left out due to large chemical shift changes induced by PGB1-QDD self-interaction (gray). Finally, the N-terminal residue is not visible in the spectra due to fast exchange with the solvent (gray). (C) Comparison of $\Delta\delta_{\mathrm{SOD1}}$ data (eq 2) at different temperatures: 10°C (dark blue), 15°C (light blue), 20°C (green), 25°C (yellow), 30°C (orange), 35°C (red), 40°C (pink), and 45°C (purple). Note that the reported values of $\Delta\delta_{\mathrm{SOD1}}$ are population-weighted averages in a sample where the concentration of PGB1-QDD is 20-fold higher than that of pwtSOD1$^{\Delta\mathrm{C}}$; at higher pwtSOD1$^{\Delta\mathrm{C}}$ concentrations, the values of $\Delta\delta_{\mathrm{SOD1}}$ are expected to be significantly higher (up to 2–4 ppm). (D) Data for $\Delta\Delta\delta = \Delta\delta_{\mathrm{SOD1}} - \Delta\delta_{\mathrm{conc}}$ (eq 2) at 20°C (black) and 45°C (red). The subtraction of $\Delta\delta_{\mathrm{conc}}$ represents a correction for concentration-dependent chemical shift changes induced by PGB1-QDD self-interaction.

reduce the noise, we characterized the chemical shift changes in BPTI by averaging data from spectra acquired at 45°C, 47°C, and 50°C (Figure 4). The resulting profile of $\Delta\delta_{\mathrm{SOD1}}$ versus BPTI sequence reveals slightly elevated values in the regions of residues 6–7, 23–25, 32–35, and 47–49.

Taken together, the chemical shift perturbations indicate that the specificity in SOD1-crowder interactions is reciprocal: inter-protein contacts appear to be more prevalent for specific regions in both pwtSOD1$^{\Delta\mathrm{C}}$ and the crowder proteins BPTI and PGB1-QDD. This result goes beyond previous conclusions reached for unfolded proteins in crowded environments,[11–14] which have not characterized the interaction surface on the crowder proteins. We presume that the specificity of these interactions is highly system dependent, as also suggested by the differential chemical shift perturbations of pwtSOD1$^{\Delta\mathrm{C}}$ upon crowding with BPTI versus PGB1-QDD.

3.3 Local Unfolding of SOD1 in MC simulations

We carried out MC simulations using a temperature, 47°C, at which SOD1 is expected to be unstable under dilute conditions. In the presence of BPTI or PGB1 crowders, it becomes even more unstable, according to the above findings. However, in our model, the folded state of

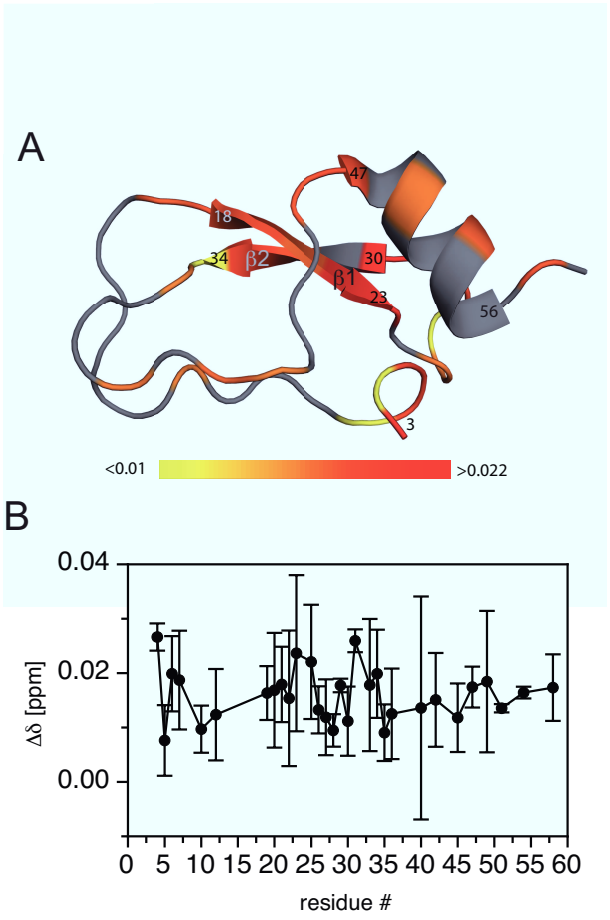

Figure 4: Chemical shift perturbations in BPTI upon interaction with pwtSOD1$^{\Delta C}$. Mean value of $\Delta\delta_{SOD1}$ (eq 2) from data acquired at 45°C, 47°C, and 50°C. (A) $\Delta\delta_{SOD1}$ values color coded on the BPTI structure (PDB-ID: 1UUA) as indicated by the color gradient at the bottom of the panel, ranging from $\Delta\delta_{SOD1} < 0.01$ ppm (yellow) to $\Delta\delta_{SOD1} > 0.022$ ppm (red). A total of 24 residues (colored gray) are left out of the analysis due to either overlap with pwtSOD1$^{\Delta C}$ resonances, missing assignments, or missing resonances (three N-terminal residues). In addition, the four proline residues are gray. (B) $\Delta\delta_{SOD1}$ values plotted as function of residue number. The error bars indicate one standard deviation, calculated from the three data sets. Assignments were obtained from BMRB entry 5359.[57]

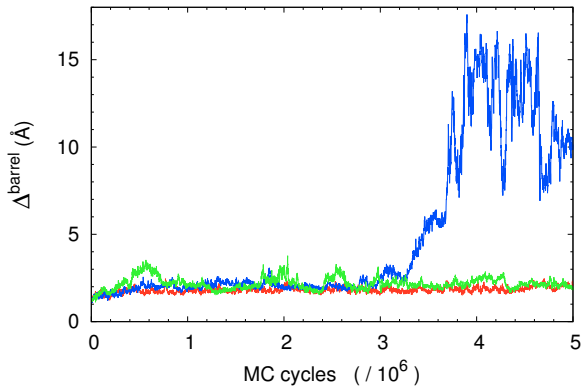

Figure 5: MC evolution of the β-barrel RMSD, Δ^{barrel}, in three simulations of the isolated SOD1 protein. In the trajectory colored red, the β-barrel stays intact throughout the entire run ($\bar{\Delta}^{\text{barrel}} < \Delta_{\text{f}}$). In the green trajectory, SOD1 visits the intermediate regime ($\Delta_{\text{f}} < \bar{\Delta}^{\text{barrel}} < \Delta_{\text{u}}$), but returns to the folded one. In the final blue trajectory, SOD1 unfolds after about 3.5×10^6 MC cycles ($\bar{\Delta}^{\text{barrel}} > \Delta_{\text{u}}$). The thresholds are set to $\Delta_{\text{f}} = 2.5$ Å and $\Delta_{\text{u}} = 5$ Å.

SOD1 remains a local free-energy minimum under all the simulated conditions, from which it may or may not escape during the course of the simulations.

To assess the foldedness of SOD1, we used as a measure the coordinate RMSD calculated over all residues in the β-barrel core, Δ^{barrel}, thus excluding the long flexible loops. To remove transient short-time fluctuations, a window-average of Δ^{barrel} is formed, called $\bar{\Delta}^{\text{barrel}}$ (see Methods). The SOD1 molecule is deemed folded (F) if $\bar{\Delta}^{\text{barrel}} < \Delta_{\text{f}}$, in an intermediate state (I) if $\Delta_{\text{f}} < \bar{\Delta}^{\text{barrel}} < \Delta_{\text{u}}$, and unfolded (U) if $\bar{\Delta}^{\text{barrel}} > \Delta_{\text{u}}$, where the thresholds are set to $\Delta_{\text{f}} = 2.5$ Å and $\Delta_{\text{u}} = 5$ Å.

Figure 5 illustrates the MC evolution of the Δ^{barrel} RMSD in 3 of our 99 runs without crowders. In one of the cases (red color), the β-barrel stays intact throughout the entire run, with $\bar{\Delta}^{\text{barrel}} < \Delta_{\text{f}}$. In another case (green), $\bar{\Delta}^{\text{barrel}}$ transiently exceeds Δ_{f}, but stays below Δ_{u} and returns to values below Δ_{f}. The third and final run (blue) contains an unfolding event, at which $\bar{\Delta}^{\text{barrel}}$ passes the unfolding threshold Δ_{u}. The fraction of all runs in which SOD1 unfolds at some point is around 30% (33% without crowders, 31% with PGB1 crowders, 27% with BPTI crowders). In none of these runs does SOD1 return to the folded regime after having unfolded. Transitions from the intermediate regime ($\Delta_{\text{f}} < \bar{\Delta}^{\text{barrel}} < \Delta_{\text{u}}$) back to the folded one do occur, as in the green trajectory of Figure 5.

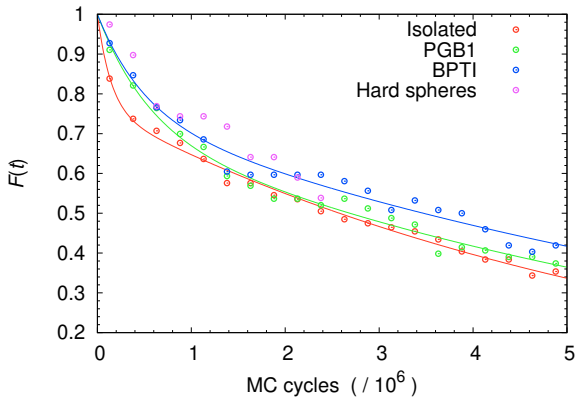

Figure 6: The fraction of runs in which the SOD1 β-barrel core is intact, $F(t)$, against MC time, as obtained without crowders (red), with PGB1 crowders (green), with BPTI crowders (blue), and with hard sphere crowders (magenta). The β-barrel is deemed intact, or folded, if $\bar{\Delta}^{\text{barrel}} < 2.5\,\text{Å}$. The curves represent fits of a simple model with the three states F, I and U, of which U is absorbing. In this model, the folded fraction is given by $F(t) = \frac{k_1 k_3}{k_+ - k_-}\left(\frac{\exp(-k_- t)}{k_- + k_1} - \frac{\exp(-k_+ t)}{k_+ + k_1}\right)$, where $k_\pm = (k_1 + k_2 + k_3)/2 \mp \sqrt{(k_1 + k_2 + k_3)^2/4 - k_1 k_2}$, k_1, k_2 and k_3 being rate constants for the reactions F→I, I→U and I→F, respectively. Our fitted values of k_1, k_2 and k_3 can be found in Table 1.

Figure 6 shows how the fraction of runs in which the β-barrel is folded ($\bar{\Delta}^{\text{barrel}} < \Delta_{\text{f}}$), $F(t)$, decays with MC time t. The decay is non-exponential, but can be quite well described in terms of a simple kinetic model with three states. The states of this model correspond to F, I and U, where U is taken to be absorbing. The model parameters are the rate constants for the reactions F→I, I→F and I→U. Although the net effects of the crowders on the decay rate of $F(t)$ are modest (Figure 6), the fitted rate constants suggest that the underlying dynamics slow down significantly when adding the crowders (Table 1); both BPTI and PGB1 crowders cause a significant reduction of all the three rate constants. The crowder-induced effects on $F(t)$ are relatively large at small t, where one of the three processes, F→I, dominates and $F(t)$ decays markedly more slowly with than without the protein crowders. A crowder-induced

Table 1: Fitted rate constants[a] of a simple three-state model (F, I, U; see Figure 6).

System	F→I	I→U	I→F
No crowders	1.79 ± 0.19	0.64 ± 0.04	4.71 ± 0.73
With PGB1 crowders	0.63 ± 0.06	0.40 ± 0.09	0.97 ± 0.24
With BPTI crowders	0.59 ± 0.07	0.41 ± 0.10	1.16 ± 0.33

[a] In $(10^6$ MC cycles$)^{-1}$.

stabilization is what one expects if the excluded-volume effect dominates, since the native state occupies less volume than the unfolded state. To judge the relative importance of the excluded-volume effect in our systems, we performed simulations with hard sphere crowders each occupying approximately the same volume as a single PGB1 or BPTI molecule. These simulations show the same qualitative behavior in MC time as those with protein crowders (Figure 6), with a similar stabilizing effect seen near the start of the simulations. This finding hints that the observed effect of the protein crowders on $F(t)$ for small t may in large part stem from steric repulsion.

The observed overall destabilization of SOD1 (Figure 2) indicates that folding becomes slower or unfolding faster in the presence of the BPTI and PGB1 crowders. The results from our unfolding simulations suggest that the primary source of destabilization is slower folding, probably caused by strong interactions between the crowders and the unfolded SOD1, as described in the previous subsection. In fact, the rate at which SOD1 unfolds in the simulations is reduced rather than enhanced when adding the crowders. This behavior is consistent with the results obtained by Linhananta et al.[58] from folding simulations of the mini-protein trp-cage. These authors found that the addition of destabilizing osmolytes led to an enhanced folding cooperativity (higher barrier).

Having studied its overall structure, we now turn to local fluctuations in the SOD1 β-barrel core. To this end, we compute two different averages of the contact-based foldedness parameter Q_k (eq 1) for each of the eight strands. The first average, referred to as "folded" and denoted by Q_k^{f}, describes the status of the strands when globally the β-barrel is in the F state or transiently in the I state. It uses all data up to and including the last time bin where $\bar{\Delta}^{\mathrm{barrel}} < \Delta_{\mathrm{f}}$ in each trajectory. The second average, referred to as "pre-unfolding" and denoted by Q_k^{pu}, describes the strands just before the β-barrel unfolds, using only data in the last time bin before $\bar{\Delta}^{\mathrm{barrel}} > \Delta_{\mathrm{u}}$ for the first time in each trajectory. Trajectories in which unfolding never occurs do not contribute to this average. Figure 7 shows our data for both Q_k^{f} and Q_k^{pu}, with and without crowders. The first average, Q_k^{f}, is high (>0.85) for all strands, as it should be. Nevertheless, there is a tendency for the strands of the first β-sheet (strands 1, 2, 3 and 6; the first four strands in each panel of Figure 7) to be slightly more intact than are those of the

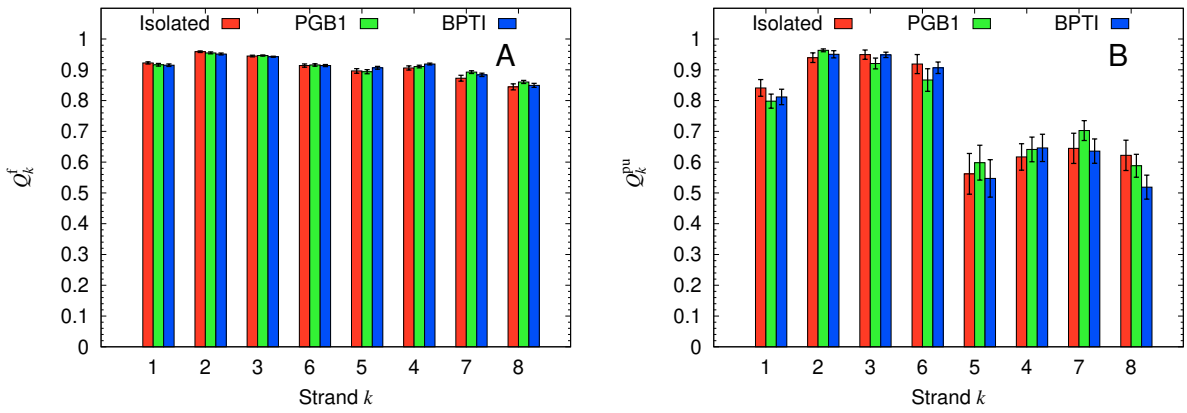

Figure 7: Foldedness of individual strands in the SOD1 β-barrel core, Q_k (eq 1), in simulations without crowders (red), with PGB1 crowders (green), and with BPTI crowders (blue). The eight strands are ordered as in the β-barrel (Figure 1). (A) "Folded" averages, Q_k^{f}, calculated using all data up to and including the last time bin where $\bar{\Delta}^{\mathrm{barrel}} < \Delta_{\mathrm{f}}$ in each trajectory. (B) "Pre-unfolding" averages, Q_k^{pu}, calculated using only data in the last time bin before $\bar{\Delta}^{\mathrm{barrel}} > \Delta_{\mathrm{u}}$ for the first time in each trajectory. Trajectories in which unfolding never occurs do not contribute to this average. The setup of our simulations is such that data collected beyond the unfolding point can be unreliable, and are therefore not considered in our analysis.

second β-sheet (strands 5, 4, 7 and 8; the last four strands in each panel of Figure 7). At a later stage, just before unfolding, this tendency becomes much stronger, as shown by the Q_k^{pu} data. The difference between the two β-sheets matches very well with experimental data[47,59] and previous simulations,[21] which have shown that the second β-sheet is more dynamic than the first.

In this context, it is worth noting that a recent study identified an aggregation-prone 11-residue segment of SOD1 capable of forming corkscrew-like oligomeric structures.[7] This segment (residues 28–38) corresponds to the β3 strand, plus one additional residue at the N-terminus and two at the C-terminus. In our simulations, the β3 strand is, along with β2, the least dynamic part of the β-barrel core. It is an open question what parts of full-length SOD1 are involved in forming oligomeric or amyloid-like structures, or whether the precursor for aggregation is a globally unfolded state[60] or a partially unfolded state.[19,21,47]

To further characterize local fluctuations in the native state of SOD1, residue-specific root-mean-square fluctuations (RMSFs) were calculated (Figure S5). The profiles of RMSF values along the amino-acid sequence match well with that of NMR order parameters previously

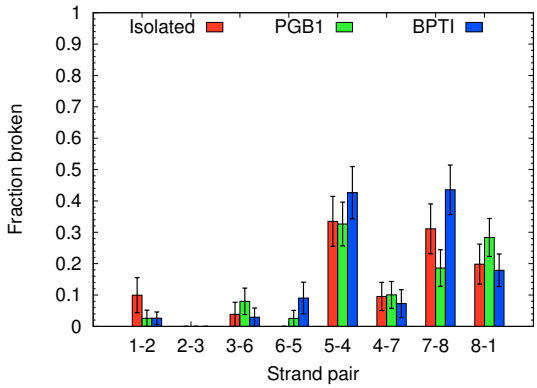

Figure 8: Probabilities of observing broken SOD1 strand pairs just before the β-barrel unfolds, in simulations without crowders (red), with PGB1 crowders (green), and with BPTI crowders (blue). The probabilities are "pre-unfolding" averages, as defined in Figure 7. A pair i, j of neighboring strands is broken if their two-strand RMSD Δ^{ij} exceeds 4 Å.

reported for apo SOD1 with the disulfide intact.[61]

It is also informative to monitor the breaking of pairs of neighboring strands in the β-barrel core. To this end, we compute a restricted two-strand RMSD, Δ^{ij}, for each of the eight pairs of neighboring strands. A pair is deemed intact if Δ^{ij} is below a threshold of 4 Å. The status of the strand pairs is evaluated just before the β-barrel unfolds, using the same kind of "pre-unfolding" average as in the calculation of Q_k^{pu}. As expected, this analysis shows (Figure 8) that pairs that tend to break early in the unfolding process involve strands from the dynamic second β-sheet. At the same time, the data show that this β-sheet unfolds in a less uniform manner than what one might guess from Figure 7. For instance, the β4-β7 pair is often intact, despite being located within the second β-sheet. To test the robustness of the findings from Figure 8, the same analysis was repeated using a similarity measure based on C_α-C_α contacts rather than on RMSD. The contact-based results (Figure S6) and are in good agreement with those in Figure 8.

In both Figures 7 and 8, the changes induced by the crowders are modest and in most cases within the statistical uncertainties. Hence, we find no indication that the interaction of SOD1 with the crowders leads to any major change in how its β-barrel core unfolds.

3.4 Simulated SOD1-Crowder Interactions

To examine the SOD1-crowder interactions, we construct residue-pair C_α-C_α contact maps. Both "folded" and "pre-unfolding" averages are formed, as in the above calculation of Q_k^{f} and Q_k^{pu} (Figure 7).

The SOD1-PGB1 and SOD1-BPTI contact maps can be found in Figures 9 and S7, respectively. These maps suggest that there exist certain interaction-prone regions on the SOD1 and crowder surfaces. On the crowders, these key regions, highlighted in blue in Figure 1, are the edge strand $\beta 2$ of PGB1 and a sticky patch on the BPTI surface, centered around residues P8 and P9. The other edge strand of PGB1, $\beta 3$, also shows some propensity to form SOD1 contacts. Interestingly, these regions of PGB1 and BPTI are largely idenical to those found prone to interact with peptides in previous work.[35–37]

These findings are in broad agreement with the chemical shift perturbation data shown in Figures 3, 4 and S3. It should be remembered, however, that the simulations cover only the early stages of the unfolding of SOD1, whereas SOD1 is substantially unfolded ($>$50%) over the entire temperature range of the NMR experiments and fully unfolded at the temperature of the MC simulations (Figure 2). The similarities in SOD1-crowder contacts observed by NMR and MC simulations suggest that the initial contacts formed during unfolding are also formed transiently under equilibrium conditions where SOD1 is unfolded.

Figures 9 and S7 show both "folded" and "pre-unfolding" averages of the contact maps. When SOD1 is folded, most of its contacts with the crowders involve the two long loops, which seem to shield the β-barrel from the surrounding crowder molecules. The number of crowder contacts is particularly low for the interior strands $\beta 4$ and $\beta 7$ of the second β-sheet, to which the long loops are anchored. When SOD1 starts unfolding, the number of contacts between its β-barrel residues and the crowders increases, as does the overall number of SOD1-crowder contacts. This trend holds with both crowders (Table 2), but is especially clear with PGB1.

In previous work,[36] we also investigated crowder-crowder contact frequencies in systems with PGB1 or BPTI as crowder protein. The amount of crowder-crowder contacts was markedly higher for BPTI than for PGB1, which is perfectly in line with the above-mentioned experimental observation that BPTI, unlike PGB1, shows a high propensity to oligomerize.

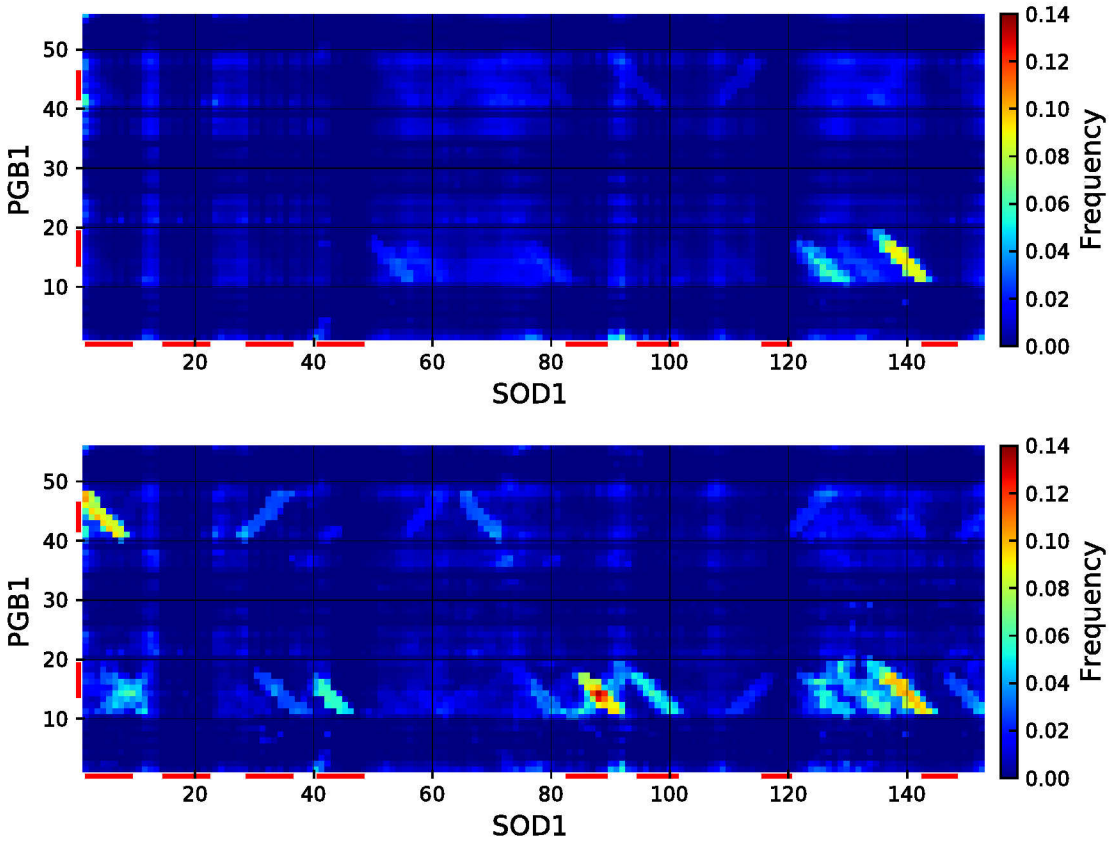

Figure 9: Simulated residue-pair contact maps for the SOD1-PGB1 system. The top and bottom panels show "folded" and "pre-unfolding" averages, respectively, as defined in Figure 7. Pixel i, j represents the average number of contacts between residue i in SOD1 and residues in position j in any of the eight PGB1 molecules. Red bars indicate the positions of all the eight strands in SOD1 and the two edge strands in PGB1. Two residues are in contact if their C_α atoms are within 8 Å from each other.

Table 2: Total numbers of residue-pair contacts with crowders formed by the full SOD1 protein and its β-barrel core, respectively, in the "folded" and "pre-unfolding" stages of the simulations.

	PGB1 crowders		BPTI crowders	
Part of SOD1	Folded[a]	Pre-unfolding[a]	Folded[a]	Pre-unfolding[a]
Full SOD1 (153 residues)	34.6 ± 1.9	48.4 ± 4.5	45.0 ± 1.7	49.3 ± 3.3
β-barrel core (57 residues)	4.2 ± 0.5	14.3 ± 2.1	5.0 ± 0.5	7.5 ± 1.3

[a] The folded and pre-unfolding stages are defined as in Figure 7.

Finally, it is worth stressing that the forces by which our two crowders act on SOD1 are different. In the SOD1-PGB1 system, the main contacts form diagonal bands (Figure 9), indicating β-structure formation, in which hydrogen bonding plays a major role . In the SOD1-BPTI system, the main contacts are between the above-mentioned sticky surface patch on BPTI and the hydrophobic 62–66 segment of the zinc-binding loop in SOD1 (Figure S7). The formation of these contacts is driven by hydrophobicity rather than by hydrogen bonding.

3.5 Simulated SOD1 Secondary-Structure Profiles

The above analysis shows that the two long loops are responsible for a large fraction of the crowder contacts formed by SOD1 in our simulations. These loops are known from experiments to be flexible under dilute conditions.[43] To examine whether the crowder interactions cause changes in the conformational preferences of the loops, we construct helix and strand probability profiles, using STRIDE secondary-structure assignments.[45]

Figure 10 shows helix and strand profiles for SOD1 in folded form in the three simulated environments. The eight strand regions can be readily identified. Outside these regions, the helix and strand probabilities vary from values close to zero up to about 0.25. Overall, the data for the three different systems are very similar, so no major crowder-induced changes occur. However, some minor changes can be seen, for instance, in the 132–137-segment of the electrostatic loop. This segment forms a short helix in the SOD1 dimer (visible in Figure 1), which can be transiently present also in the apo-reduced monomer with mainly flexible loops.[43] Consistent with this, without crowders, our simulated helix probability profile (Figure 10) exhibits a local maximum in the 132–137-region. When adding crowders, this peak becomes higher,

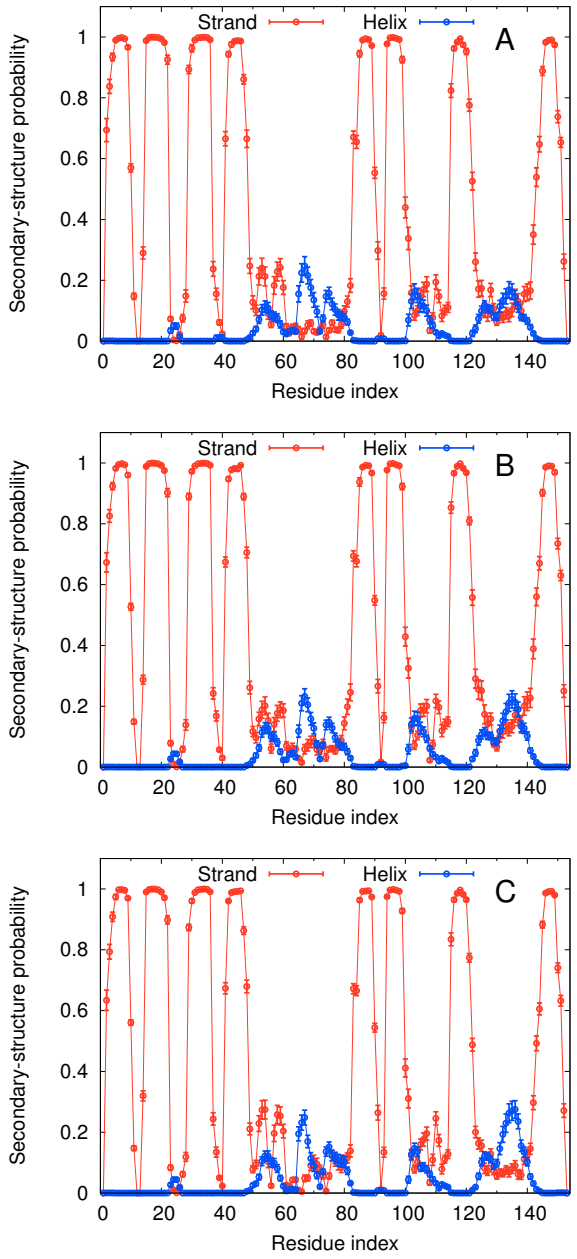

Figure 10: Strand and helix probability profiles for folded SOD1, as obtained from simulations (A) without crowders, (B) with PGB1 crowders, and (C) with BPTI crowders. The probabilities are "folded" averages, as defined in Figure 7. Secondary structure is assigned using STRIDE.[45]

especially in the BPTI case. Our simulations thus indicate that the propensity of the 132–137 segment to form a helix increases upon the addition of the crowders.

Figure S8 shows "pre-unfolding" secondary-structure profiles, which are noisier, due to limited statistics. Nevertheless, the strand profiles in this figure support the conclusion that the second β-sheet is less stable than the first (Figure 7). A comparison with the secondary-structure profiles for folded SOD1 (Figure 10) furthermore hints at a tendency for the helix and strand probabilities in the loop regions to increase as the β-barrel unfolds.

4 Conclusions

In this article, we have combined NMR and MC methods to investigate how SOD1, in its disulfide-reduced apo monomeric form, is affected by the presence of BPTI and PGB1 crowders. Our NMR experiments show that both crowders, and especially BPTI, cause a drastic reduction of the overall stability of SOD1. Furthermore, we acquired chemical shift data that provide residue-level information on how PGB1 and BPTI interact with SOD1.

Our MC simulations focused on the early stages in thermal unfolding of SOD1. Fits of a simple three-state model (F, I, U) indicate that the SOD1 dynamics become slower in the presence of the crowders. However, we observed no major crowder-induced changes in the net decay rate of the β-barrel core, or in how this structure unfolds. Both with and without crowders, we find that the second β-sheet is more unfolding-prone than the first, as observed in previous experiments under crowder-free conditions.[47,59] The observation that the crowders do not facilitate unfolding in the simulations hints that the primary reason for the observed destabilization of SOD1 is slower folding, presumably caused by strong interactions between the crowders and the unfolded SOD1. This conclusion is in full agreement with our NMR results.

Both the simulated residue-pair contact maps and the NMR chemical shift perturbations reveal that the interaction propensities are far from uniform over the SOD1 and crowder protein surfaces. Interestingly, the identification of crowder residues prone to interact with SOD1 in the unfolding simulations is in broad agreement with the NMR measurements (under equilibrium

conditions). This agreement indicates that key contacts stabilizing the unfolded state of SOD1 may form early in the unfolding process.

Acknowledgement

This work was in part supported by the Swedish Research Council (Grant nos. 621-2014-4522 and 621-2014-5815). KSJ holds a grant from the Danish Council for Independent Research, Sapere Aude: DFF-Research Talent (Grant no. 4002-00258). The simulations were performed on resources provided by the Swedish National Infrastructure for Computing (SNIC) at LUNARC, Lund University, Sweden, and Jülich Supercomputing Centre, Forschungszentrum Jülich, Germany. We thank Bertil Halle for the BPTI sample and Johan Wallerstein for the ^{13}C,^{15}N-PGB1 sample.

Supporting Information Available

The Supporting Information is available free of charge.

Figure S1, folded population of pwtSOD1$^{\Delta C}$ in the presence of PGB1-QDD crowders as estimated from NMR cross peaks of the C-terminal Q153 residue and the W32 side chain, respectively; Figure S2, chemical shift perturbations in the native fraction of pwtSOD1$^{\Delta C}$ upon interaction with PGB1; Figure S3, HSQC NMR spectra for pwtSOD1$^{\Delta C}$ with and without crowders; Figure S4, chemical shift perturbations in PGB1-QDD solutions upon dilution; Figure S5, simulated RMSF profiles; Figure S6, same as Figure 8 but based on C_α-C_α contacts rather than on RMSD; Figure S7, simulated residue-pair contact maps for the SOD1-BPTI system; Figure S8, simulated secondary-structure profiles for SOD1 just before unfolding.

References

(1) Rosen, D. R.; Siddique, T.; Patterson, D.; Figlewicz, D. A.; Sapp, P.; Hentati, A.; Donaldson, D.; Goto, J.; O'Regan, J. P.; Deng, H. X. et al. Mutations in Cu/Zn superoxide

dismutase gene are associated with familial amyotrophic lateral sclerosis. *Nature* **1993**, *362*, 59–62.

(2) Cleveland, D. W.; Rothstein, J. D. From Charcot to Lou Gehrig: deciphering selective motor neuron death in ALS. *Nat. Rev. Neurosci.* **2001**, *2*, 806–819.

(3) Valentine, J. S.; Doucette, P. A.; Potter, S. Z. Copper-zinc superoxide dismutase and amyotrophic lateral sclerosis. *Annu. Rev. Biochem.* **2005**, *74*, 563–593.

(4) Robberecht, W.; Philips, T. The changing scene of amyotrophic lateral sclerosis. *Nat. Rev. Neurosci.* **2013**, *14*, 248–264.

(5) Mulligan, V. K.; Chakrabartty, A. Protein misfolding in the late-onset neurodegenerative diseases: common themes and the unique case of amyotrophic lateral sclerosis. *Proteins* **2013**, *81*, 1285–1303.

(6) Proctor, E. A.; Fee, L.; Tao, Y.; Redler, R. L.; Fay, J. M.; Zhang, Y.; Lv, Z.; Mercer, I. P.; Deshmukh, M.; Lyubchenko, Y. L. et al. Nonnative SOD1 trimer is toxic to motor neurons in a model of amyotrophic lateral sclerosis. *Proc. Natl. Acad. Sci. USA* **2016**, *113*, 614–619.

(7) Sangwan, S.; Zhao, A.; Adams, K. L.; Jayson, C. K.; Sawaya, M. R.; Guenther, E. L.; Pan, A. C.; Ngo, J.; Moore, D. M.; Soriaga, A. B. et al. Atomic structure of a toxic, oligomeric segment of SOD1 linked to amyotrophic lateral sclerosis (ALS). *Proc. Natl. Acad. Sci. USA* **2017**, *114*, 8770–8775.

(8) Rodriguez, J. A.; Shaw, B. F.; Durazo, A.; Sohn, S. H.; Doucette, P. A.; Nersissian, A. M.; Faull, K. F.; Eggers, D. K.; Tiwari, A.; Hayward, L. J. Destabilization of apoprotein is insufficient to explain Cu, Zn-superoxide dismutase linked ALS pathogenesis. *Proc. Natl. Acad. Sci. USA* **2005**, *102*, 10516–10521.

(9) Vassall, K. A.; Stubbs, H. R.; Primmer, H. A.; Tong, M. S.; Sullivan, S. M.; Sobering, R.; Srinivasan, S.; Briere, L.-A. K.; Dunn, S. D.; Colón, W. et al. Decreased stability and

increased formation of soluble aggregates by immature superoxide dismutase do not account for disease severity in ALS. *Proc. Natl. Acad. Sci. USA* **2011**, *108*, 2210–2215.

(10) Luchinat, E.; Barbieri, L.; Rubino, J. T.; Kozyreva, T.; Cantini, F.; Banci, L. In-cell NMR reveals potential precursor of toxic species from SOD1 fALS mutants. *Nat. Comm.* **2014**, *5*, 5502.

(11) Danielsson, J.; Mu, X.; Lang, L.; Wang, H.; Binolfi, A.; Theillet, F.-X.; Bekei, B.; Logan, D. T.; Selenko, P.; Wennerström, H. et al. Thermodynamics of protein destabilization in live cells. *Proc. Natl. Acad. Sci. USA* **2015**, *112*, 12402–12407.

(12) Miklos, A. C.; Sarkar, M.; Wang, Y.; Pielak, G. J. Protein crowding tunes protein stability. *J. Am. Chem. Soc.* **2011**, *133*, 7116–7120.

(13) Harada, R.; Tochio, N.; Kigawa, T.; Sugita, Y.; Feig, M. Reduced native state stability in crowded cellular environment due to protein–protein interactions. *J. Am. Chem. Soc.* **2013**, *135*, 3696–3701.

(14) Monteith, W. B.; Pielak, G. J. Residue level quantification of protein stability in living cells. *Proc. Natl. Acad. Sci. USA* **2014**, *111*, 11335–11340.

(15) Shen, J.; Subramaniam, S.; Wong, C. F.; McCammon, J. A. Superoxide dismutase: fluctuations in the structure and solvation of the active site channel studied by molecular dynamics simulation. *Biopolymers* **1989**, *28*, 2085–2096.

(16) Strange, R. W.; Yong, C. W.; Smith, W.; Hasnain, S. S. Molecular dynamics using atomic-resolution structure reveal structural fluctuations that may lead to polymerization of human Cu-Zn superoxide dismutase. *Proc. Natl. Acad. Sci. USA* **2007**, *104*, 10040–10044.

(17) Schmidlin, T.; Kennedy, B. K.; Daggett, V. Structural changes to monomeric CuZn superoxide dismutase caused by the familial amyotrophic lateral sclerosis-associated mutation A4V. *Biophys. J.* **2009**, *97*, 1709–1718.

(18) Kumar, V.; Prakash, A.; Lynn, A. Alterations in local stability and dynamics of A4V SOD1 in the presence of trifluoroethanol. *Biopolymers* **2018**, *362*, e23102.

(19) Ding, F.; Dokholyan, N. V. Dynamical roles of metal ions and the disulfide bond in Cu, Zn superoxide dismutase folding and aggregation. *Proc. Natl. Acad. Sci. USA* **2008**, *105*, 19696–19701.

(20) Proctor, E. A.; Ding, F.; Dokholyan, N. V. Structural and thermodynamic effects of post-translational modifications in mutant and wild type Cu, Zn superoxide dismutase. *J. Mol. Biol.* **2011**, *408*, 555–567.

(21) Ding, F.; Furukawa, Y.; Nukina, N.; Dokholyan, N. V. Local unfolding of Cu, Zn superoxide dismutase monomer determines the morphology of fibrillar aggregates. *J. Mol. Biol.* **2012**, *421*, 548–560.

(22) Bille, A.; Jónsson, S. Æ.; Akke, M.; Irbäck, A. Local unfolding and aggregation mechanisms of SOD1: a Monte Carlo exploration. *J. Phys. Chem. B* **2013**, *117*, 9194–9202.

(23) Das, A.; Plotkin, S. S. Mechanical probes of SOD1 predict systematic trends in metal and dimer affinity of ALS-associated mutants. *J. Mol. Biol.* **2013**, *425*, 850–874.

(24) Das, A.; Plotkin, S. S. SOD1 exhibits allosteric frustration to facilitate metal binding affinity. *Proc. Natl. Acad. Sci. USA* **2013**, *110*, 3871–3876.

(25) Habibi, M.; Plotkin, S. S.; Rottler, J. Soft vibrational modes predict breaking events during force-induced protein unfolding. *Biophys. J.* **2018**, *114*, 562–569.

(26) Harder, T.; Borg, M.; Bottaro, S.; Boomsma, W.; Olsson, S.; Ferkinghoff-Borg, J.; Hamelryck, T. An efficient null model for conformational fluctuations in proteins. *Structure* **2012**, *20*, 1028–1039.

(27) Delano, W. L. *The PyMOL Molecular Graphics System*; DeLano Scientific: Palo Alto, CA, 2002.

(28) Vendeville, A.; Larivière, D.; Fourmentin, E. An inventory of the bacterial macromolecular components and their spatial organization. *FEMS Microbiol. Rev.* **2011**, *35*, 395–414.

(29) Irbäck, A.; Mitternacht, S.; Mohanty, S. An effective all-atom potential for proteins. *BMC Biophys.* **2009**, *2*, 2.

(30) Mitternacht, S.; Luccioli, S.; Torcini, A.; Imparato, A.; Irbäck, A. Changing the mechanical unfolding pathway of FnIII-10 by tuning the pulling strength. *Biophys. J.* **2009**, *96*, 429–441.

(31) Jónsson, S. Æ.; Mohanty, S.; Irbäck, A. Distinct phases of free α-synuclein — a Monte Carlo study. *Proteins* **2012**, *80*, 2169–2177.

(32) Mohanty, S.; Meinke, J. H.; Zimmermann, O. Folding of Top7 in unbiased all-atom Monte Carlo simulations. *Proteins* **2013**, *81*, 1446–1456.

(33) Jónsson, S. Æ.; Mitternacht, S.; Irbäck, A. Mechanical resistance in unstructured proteins. *Biophys. J.* **2013**, *104*, 2725–2732.

(34) Petrlova, J.; Bhattacherjee, A.; Boomsma, W.; Wallin, S.; Lagerstedt, J. O.; Irbäck, A. Conformational and aggregation properties of the 1–93 fragment of apolipoprotein A-I. *Protein Sci.* **2014**, *23*, 1559–1571.

(35) Bille, A.; Linse, B.; Mohanty, S.; Irbäck, A. Equilibrium simulation of trp-cage in the presence of protein crowders. *J. Chem. Phys.* **2015**, *143*, 175102.

(36) Bille, A.; Mohanty, S.; Irbäck, A. Peptide folding in the presence of interacting protein crowders. *J. Chem. Phys.* **2016**, *144*, 175105.

(37) Nilsson, D.; Mohanty, S.; Irbäck, A. Markov modeling of peptide folding in the presence of protein crowders. *J. Chem. Phys.* **2018**, *148*, 055101.

(38) Moses, E.; Hinz, H.-J. Basic pancreatic trypsin inhibitor has unusual thermodynamic stability parameters. *J. Mol. Biol.* **1983**, *170*, 765–776.

(39) Gronenborn, A. M.; Filpula, D. R.; Essig, N. Z.; Achari, A.; Whitlow, M.; Wingfield, P. T.; Clore, G. M. A novel, highly stable fold of the immunoglobulin binding domain of streptococcal protein G. *Science* **1991**, *253*, 657–661.

(40) Tiana, G.; Sutto, L.; Broglia, R. A. Use of the Metropolis algorithm to simulate the dynamics of protein chains. *Physica A* **2007**, *380*, 241–249.

(41) Favrin, G.; Irbäck, A.; Sjunnesson, F. Monte Carlo update for chain molecules: Biased Gaussian steps in torsional space. *J. Chem. Phys.* **2001**, *114*, 8154–8158.

(42) Irbäck, A.; Mohanty, S. PROFASI: a Monte Carlo simulation package for protein folding and aggregation. *J. Comput. Chem.* **2006**, *27*, 1548–1555.

(43) Sekhar, A.; Rumfeldt, J. A. O.; Broom, H. R.; Doyle, C. M.; Bouvignies, G.; Meiering, E. M.; Kay, L. E. Thermal fluctuations of immature SOD1 lead to separate folding and misfolding pathways. *eLife* **2015**, *4*, e07296.

(44) Chikenji, G.; Fujitsuka, Y.; Takada, S. Protein folding mechanisms and energy landscape of src SH3 domain studied by a structure prediction toolbox. *Chem. Phys.* **2004**, *307*, 157–162.

(45) Frishman, D.; Argos, P. Knowledge-based protein secondary structure assignment. *Proteins* **1995**, *23*, 566–579.

(46) Khan, M. A. I.; Respondek, M.; Kjellström, S.; Deep, S.; Linse, S.; Akke, M. Cu/Zn superoxide dismutase forms amyloid fibrils under near-physiological quiescent conditions: the roles of disulfide bonds and effects of denaturant. *ACS Chem. Neurosci.* **2017**, *8*, 2019–2026.

(47) Teilum, K.; Smith, M. H.; Schulz, E.; Christensen, L. C.; Solomentsev, G.; Oliveberg, M.; Akke, M. Transient structural distortion of metal-free Cu/Zn superoxide dismutase triggers aberrant oligomerization. *Proc. Natl. Acad. Sci. USA* **2009**, *106*, 18273–18278.

(48) Lindman, S.; Xue, W. F.; Szczepankiewicz, O.; Bauer, M. C.; Nilsson, H.; Linse, S. Salting the charged surface: pH and salt dependence of protein G B1 stability. *Biophys. J.* **2006**, *90*, 2911–2921.

(49) Wallerstein, J.; Weininger, U.; Khan, M. A.; Linse, S.; Akke, M. Site-specific protonation kinetics of acidic side chains in proteins determined by pH-dependent carboxyl ^{13}C NMR relaxation. *J. Am. Chem. Soc.* **2015**, *137*, 3093–3101.

(50) Delaglio, F.; Grzesiek, S.; Vuister, G. W.; Zhu, G.; Pfeifer, J.; Bax, A. NMRPipe: a multidimensional spectral processing system based on UNIX pipes. *J. Biomol. NMR* **1995**, *6*, 277–293.

(51) Vranken, W. F.; Boucher, W.; Stevens, T. J.; Fogh, R. H.; Pajon, A.; Llinas, P.; Ulrich, E. L.; Markley, J. L.; Ionides, J.; Laue, E. D. The CCPN data model for NMR spectroscopy: development of a software pipeline. *Proteins* **2005**, *59*, 687–696.

(52) Gottschalk, M.; Venu, K.; Halle, B. Protein self-association in solution: the bovine pancreatic trypsin inhibitor decamer. *Biophys. J.* **2003**, *84*, 3941–3958.

(53) Snoussi, K.; Halle, B. Protein self-association induced by macromolecular crowding: a quantitative analysis by magnetic relaxation dispersion. *Biophys. J.* **2005**, *88*, 2855–2866.

(54) Williamson, M. P. Using chemical shift perturbation to characterise ligand binding. *Prog. Nucl. Magn. Reson. Spectrosc.* **2013**, *73*, 1–16.

(55) Schwarzinger, S.; Kroon, G. J. A.; Foss, T. R.; Wright, P. E.; Dyson, H. J. Random coil chemical shifts in acidic 8 M urea: implementation of random coil shift data in NMRView. *J. Biomol. NMR* **2000**, *18*, 43–48.

(56) Lindman, S.; Bauer, M. C.; Lund, M.; Diehl, C.; Mulder, F. A. A.; Akke, M.; Linse, S. pK_a values for the unfolded state under native conditions explain the pH-dependent stability of PGB1. *Biophys. J.* **2010**, *99*, 3365–3373.

(57) Biamonti, C. Structural and dynamic investigations of macromolecular recognition processes by nuclear magnetic resonance spectroscopy. Ph.D. thesis, Rutgers University, 1996.

(58) Linhananta, A.; Hadizadeh, S.; Plotkin, S. S. An effective solvent theory connecting the underlying mechanisms of osmolytes and denaturants for protein stability. *Biophys. J.* **2011**, *100*, 459–468.

(59) Doyle, C. M.; Rumfeldt, J. A.; Broom, H. R.; Sekhar, A.; Kay, L. E.; Meiering, E. M. Concurrent increases and decreases in local stability and conformational heterogeneity in Cu, Zn superoxide dismutase variants revealed by temperature-dependence of amide chemical shifts. *Biochemistry* **2016**, *55*, 1346–1361.

(60) Lang, L.; Kurnik, M.; Danielsson, J.; Oliveberg, M. Fibrillation precursor of superoxide dismutase 1 revealed by gradual tuning of the protein-folding equilibrium. *Proc. Natl. Acad. Sci. USA* **2012**, *109*, 17868–17873.

(61) Banci, L.; Bertini, I.; Cramaro, F.; Del Conte, R.; Viezzoli, M. S. Solution structure of apo Cu,Zn superoxide dismutase: role of metal ions in protein folding. *Biochemistry* **2003**, *42*, 9543–9553.

TOC Graphic